THE JOURNAL OF PHYSICAL CHEMISTRY C

ARTICLE

pubs.acs.org/JPCC

Effect of Single Femtosecond Pulses on Gold Nanoparticles

Omri Warshavski, Limor Minai, Gili Bisker, and Dvir Yelin*

Department of Biomedical Engineering, Technion − Israel Institute of Technology, 32000 Haifa, Israel

ABSTRACT: Gold nanoparticles find a wide range of applications in optics and photonics; however, their detailed interaction with intense laser light is only partially understood. Previous works have studied the effect of intense pulse trains on gold nanoparticles at a wide range of illumination parameters and observed diverse optical and morphological changes. In this work we study, for the first time, the interaction between single femtosecond pulses and gold nanoparticles. Using transmission electron microcopy and optical spectroscopy, we have found that nanoparticles illuminated by 50 fs pulses with fluence of less than 0.15 J/cm^2 per pulse (3 TW/cm^2) undergo morphological changes that affect their extinction spectra. Experimentation with particles of different diameters show similar qualitative effects, which are more pronounced for larger particles. Pulses at different excitation wavelengths were found to induce different effects for resonance and off-resonance conditions. The presented results provide valuable experimental data on the complex pulse−particle interaction and would be helpful for better understanding of the physical processes that are involved.

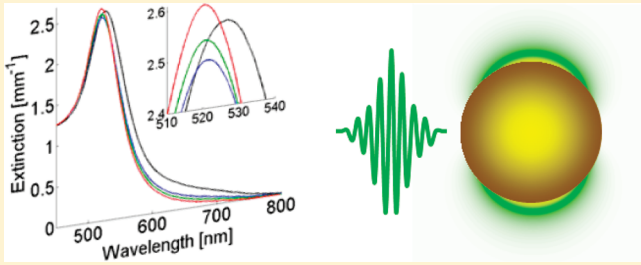

INTRODUCTION

Owing to their unique optical properties, gold nanoparticles (GNPs) have a wide range of applications in biology and biomedicine,[1−3] including nonlinear microscopy,[4−6] single molecule sensing,[7,8] DNA sequencing,[9] photoactivated therapeutics,[10,11] and targeted thermal therapy.[12−14] Perhaps the most unique feature of GNPs is their strong plasmonic resonance, a collective oscillation of the conduction electrons driven by an external electromagnetic field in the visible or the near-infrared parts of the spectrum. At resonance, the absorption and scattering cross sections of the particles increase dramatically, and the local electromagnetic fields at close proximity to the surface of the particles are strongly enhanced. The wavelengths at which resonance excitations occur depend on the shape and size of the nanoparticles, as well as on the dielectric constants of the particles and their surrounding medium.[15−17]

When light intensities reach certain threshold levels, for example by illuminating the nanoparticles with ultrashort laser pulses, structural modifications of the nanoparticles take place, which alter their morphology and consequently their optical properties. Such effects strongly depend on pulse energy, peak intensity, wavelength, and pulse duration. Structural modifications of GNPs were experimentally observed following their illumination by nanosecond and picosecond pulses at resonance[18−23] and off-resonance[23,24] wavelengths and were mainly attributed to processes such as particle melting and coulomb explosions. The interaction between GNPs and pulses in the femtosecond range typically involves additional mechanisms owing to their orders-of-magnitude higher intensities and the short interaction time scales.[25,26] Even without the presence of nanoparticles, high-intensity femtosecond pulses were shown to induce a wide variety of processes in water, including photoionization, cascade ionization, formation of reactive oxygen species, creation of cavitation bubbles, and rapid temperature increase.[27] With nanoparticles present at the focal volume of a femtosecond beam, a wider variety of phenomena may occur due to the additional interaction of the pulse with the particles.[28−33] In gold nanorods,[1,34] several research groups have reported changes in the extinction spectra and in particle morphology following exposure to femtosecond pulses at near-infrared resonance wavelengths under various conditions. The observed changes include superheating of the nanorods, fragmentation, particle melting, and surface melting.[20] The apparent spectral hole burning[20] was attributed mainly to the conversion of the nanorods into nanospheres, which are more structurally stable. Despite the extensive experimental and theoretical research, the detailed mechanisms by which intense light affects the particles and their close environment are not entirely understood. Clearly, separating the effect of a single pulse from that of a long series of pulses could be utilized to isolate and identify the exact processes which are involved. Recently, the effect of a single 10 ns pulse at a wavelength of 532 nm, which closely matches the absorption resonance of the illuminated gold nanospheres, was found to include particle ionization followed by fragmentation due to coulomb explosions.[21,24,35] To the best of our knowledge, the effect of a single femtosecond pulse on noble-metal nanoparticles, both at resonance and off-resonance wavelengths, has not been experimentally studied.

In this work, we experimentally investigated the optical and morphological effects of single femtosecond pulses on gold

Received: October 29, 2010
Revised: January 12, 2011
Published: February 18, 2011

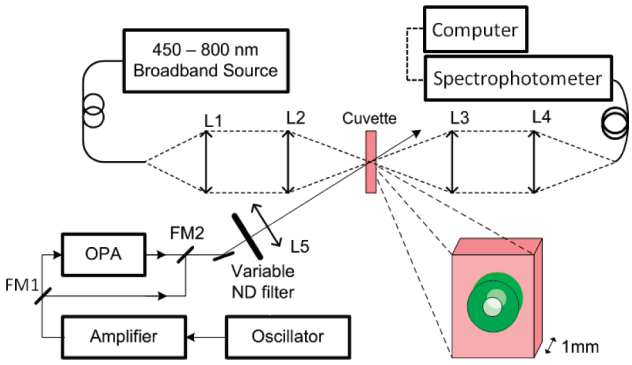

Figure 1. Schematic of the optical setup. Green and white circles on the cuvette represent the cross sections of the high-intensity pulse beam and the probe beam, respectively. L1−L5: lenses. FM1, FM2: Flip mirrors. ND: Neutral density. OPA: Optical parametric amplifier.

nanoparticles. First, we identified and characterized changes in the extinction spectra of three different particle solutions illuminated by single pulses of different intensities and at two excitation wavelengths: one at 550 nm, corresponding to the resonance excitation conditions of the particles, the other at 800 nm, corresponding to off-resonance excitation. The illuminated nanoparticles were then imaged using transmission electron microscopy (TEM). Morphological and statistical data from the TEM images were collected, analyzed, and compared to the corresponding spectral changes.

EXPERIMENTAL METHODS

Gold nanoparticles were prepared using a seeding growth method[36,37] in which small particles (3−5 nm) were used as nucleation centers for the production of larger nanospheres. The final particle size was adjusted by controlling the relative concentration of the seeds and the added growth solution containing gold salt. To prevent particles aggregation, 1 mM of cetyltrimethylammonium bromide (CTAB) was included in the growth solution. Further enlargement of the particles was achieved using the resulting particles as seeds for the next growth phase. Three different particle solutions resulting from three consecutive growth phases were imaged by TEM (Tecnai Inc. G2 T20, 200 kV) to determine particle size and shape distributions. The effective diameter d_S of each particle in the TEM images was calculated according to $d_S = 2(S/\pi)^{1/2}$, where S denotes the measured area of the particle in the 2D TEM image. The particle solutions which were chosen for the experiments had average particle diameters of 16, 23, and 45 nm and are referred to as GNP-16, GNP-23, and GNP-45, respectively, throughout the text.

The particle solutions which were used for the experiments were centrifuge-concentrated (13K rpm, 15 min) to approximately 5×10^{10} particles/ml. The nearly identical extinction spectra measured before and after centrifugation confirmed that no significant aggregation has occurred during the process. Sample preparation for the TEM was accomplished by placing 2 μL of the solutions on carbon-coated copper grids, followed by 10 h drying in vacuum. To minimize calibration errors, all TEM photographs used for data analysis were taken at constant magnification.

To study the effect of femtosecond pulses on the gold nanoparticles, a portion of each solution was placed in a 1 mm thick rectangular glass cuvette, which was placed at the focal plane of an optical arrangement (Figure 1). This experimental setup allowed the illumination of the particles with single pulses while observing changes in the extinction spectra. Light from a visible broadband source (Oriel instruments, Apex fiber illuminator, 50 W quartz tungsten halogen lamp) was coupled into a multimode optical fiber (200 μm core diameter) whose distal end was imaged into a 133 μm diameter spot on the cuvette using two achromatic lenses L1 (75 mm focal length) and L2 (50 mm focal length). The focal depth was approximately 5 mm, longer than the total cuvette thickness (1 mm). The light transmitted through the cuvette was then collimated (lens L3, 75 mm focal length) and refocused (lens L4, 150 mm focal length) into a multimode fiber (600 μm core diameter), which was used as the input of a commercial spectrophotometer (Ocean Optics Inc., USB4000) having a maximal capturing rate of 250 spectra per second. The wavelength-dependent extinction coefficients were computed by taking the logarithm of the ratio between the transmitted spectra of pure water and that of the nanoparticle solution.

In many applications of gold nanoparticles, optical and photochemical effects are most effectively generated by high field intensities. Such applications include nonlinear microscopy,[4−6] surface-enhanced Raman scattering,[8,40] material nanoprocessing,[31−33] and nanosurgery.[41] It has been shown[16] that the wavelength that causes maximum near-field enhancement is somewhat red-shifted from the wavelength of maximum extinction. The averaged near-field intensities on the surface of nanospheres with diameters of 16, 23, and 45 nm, calculated based on the Mie theory,[16] showed maxima at approximately 550 nm for all particle diameters, red-shifted by approximately 15 nm from the measured extinction maxima (data not shown). Therefore, to effectively enhance intensity-related processes in the particles and their close vicinity, we have chosen to use the wavelength of 550 nm for our resonant illumination experiments.

On-resonance high-intensity pulse illumination was achieved by aiming a beam of approximately 50 fs pulses from an optical parametric amplifier (OPA, Spectra-Physics, Topas) pumped by a Ti:Sapphire amplifier (Spectra-Physics, Spitfire Pro XP) at the face of the cuvette, where the center of the laser spot coincided with the center of the white light probe beam (Figure 1). The maximum pulse rate of the system was 1 kHz, however during all our experiments we have used a single pulse mode of the system, in which single pulses can be triggered manually. The OPA central wavelength was tuned to match the resonance frequency for maximum near field enhancement (550 nm), with approximately 0.3 mJ per pulse. Off-resonance illumination at 800 nm was achieved by aiming the beam directly from the amplifier (50 fs pulse duration, 3 mJ per pulse), using flip mirrors FM1 and FM2.

For both excitation wavelengths, pulse intensity was adjusted by sliding a lens (L5, 400 mm focal length) along its optical axis, allowing continuous adjustment of the beam diameter on the cuvette between 0.6 mm and 1.5 mm, which corresponded to a fluence of up to 0.15 J/cm^2 and peak intensities of up to 3 TW/cm^2. Lower pulse intensities were achieved using a variable neutral density (ND) filter before the lens L5. During the experiments, the diameter of the pulse beam on the cuvette was kept larger than that of the probe beam (133 μm), ensuring that extinction spectra were measured only for particles that were exposed to the high-intensity pulses.

RESULTS

The extinction spectra of the GNP-16, GNP-23, and the GNP-45 solutions following illumination of single 50 fs pulses of 90

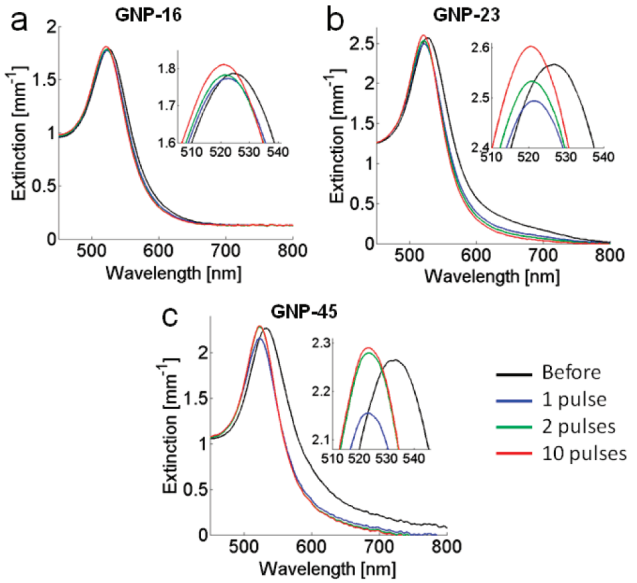

Figure 2. On-resonance (550 nm) illumination. Extinction spectra of the solutions (a) GNP-16, (b) GNP-23, and (c) GNP-45 illuminated by femtosecond pulses at 550 nm.

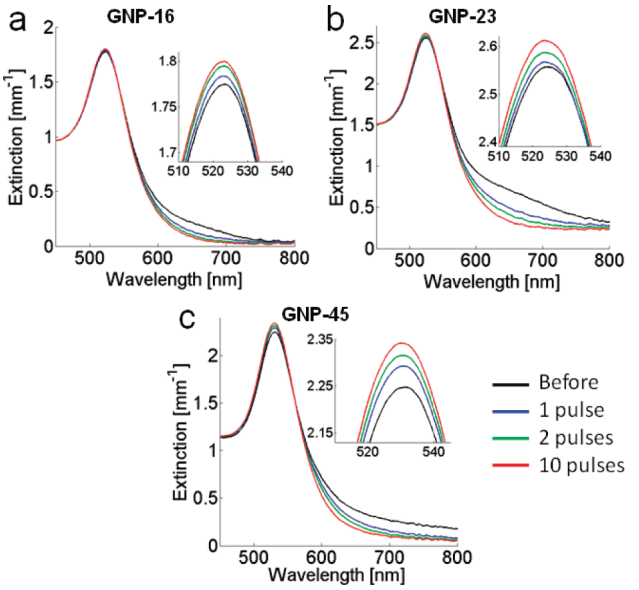

Figure 3. Off-resonance (800 nm) illumination. Extinction spectra of the solutions (a) GNP-16, (b) GNP-23, and (c) GNP-45 illuminated by femtosecond pulses at 800 nm.

mJ/cm^2 per pulse (1.8 TW/cm^2), at a center wavelength of 550 nm, are shown in parts a, b, and c respectively of Figure 2. A comparison between the extinction spectra before illumination (black line) and immediately after (less than a second) 1 pulse (blue), 2 pulses (green), and 10 pulses (red) reveal noticeable differences in the extinction spectra after each pulse. The effect of the first pulse was the most significant for all three solutions, and included noticeable blue shifts of the spectra, spectral narrowing by 5−25%, decrease in the maximum extinction values by approximately 5%, and a substantial decrease of the extinction at near-infrared wavelengths by 70−90%. The effect of the second pulse was less pronounced but had a similar trend, with the exception of the peak extinction values which slightly increased compared to the peak values after 1 pulse. Similar effects, although gradually decreasing in magnitudes, were observed after each additional pulse, until no changes were visible after more than 10 pulses. The above spectral changes were found to be independent of the temporal separation between pulses, which was approximately 1 s throughout the experiment. At pulse delays longer than a few tens of seconds, though, the measurement was affected by diffusion of nonilluminated particles into the measured volume.

Because the near field enhancement and the absorption cross-section drop significantly at 800 nm, the overall effect of a single pulse at 800 nm is expected to be smaller compared with resonance excitation. To study this effect, the three nanoparticle solutions were illuminated with 50 fs pulses from the Ti:Sapphire amplifier, with 800 nm central wavelength and pulse energy of approximately 3 mJ, corresponding to fluence of 0.15 J/cm^2 and peak intensity of 3 TW/cm^2 (66% higher than in the resonance illumination experiment described previously). The extinction spectra acquired after pulse illumination of the GNP-16, GNP-23, and GNP-45 solutions are shown in parts a, b, and c respectively of Figure 3. In contrast to resonant illumination with 550 nm, a comparison between the extinction spectra before illumination (black line) and immediately after 1 pulse (blue), 2 pulses (green), and 10 pulses (red) revealed a small but consistent increase in peak extinction after each pulse, and less than 1 nm total blue shift of the peak extinction wavelength. More noticeable was the decrease of the extinction coefficient at wavelengths longer than 600 nm. Similar spectral hole burning was previously observed in high aspect ratio particles using a long train of femtosecond pulses.[20,42] For all three solutions, the effect of the first pulse was only slightly more pronounced than that of the following ones. No significant changes were observed after more than 10 pulses. Here, too, the observed spectral changes were found to be independent of the time gaps between the pulses.

To quantify the role of pulse intensity in the observed effects, the GNP-45 solution was illuminated at resonance (550 nm) wavelength by either a single pulse or 10 pulses with increasing pulse intensities, whereas the extinction spectra were recorded before and after illumination. The blue shifts of the peak extinction wavelength $\Delta\lambda_{peak}$ (part a of Figure 4) after a single pulse (full diamonds) and 10 pulses (empty diamonds) reveal that the effect becomes pronounced only above a threshold intensity of approximately 420 GW/cm^2. To compare the threshold intensities between resonance (550 nm) and off-resonance (800 nm) excitation, different parameters must have been chosen because the blue spectral shift at off-resonance illumination was too small to be used as an effective parameter. Instead, we have chosen the extinction decrease at the wavelength of 650 nm, denoted by $\Delta\mu_{650}$, as a parameter that best describes most of the observed spectral changes. Plots of $\Delta\mu_{650}$ for different pulse intensities following resonance (green markers) and off-resonance (red markers) excitation by 1 pulse (full markers) and 10 pulses (empty markers) are shown in part b of Figure 4. The plots show the existence of threshold intensities for both wavelengths (400 GW/cm^2 and 800 GW/cm^2 for resonance and off-resonance illumination, respectively) with different transition slopes, which indicates that the underlying physical effect was different between resonance and off-resonance excitation.

The extinction parameters shown in Figures 2−4 indicate that certain structural and morphological parameters were changed

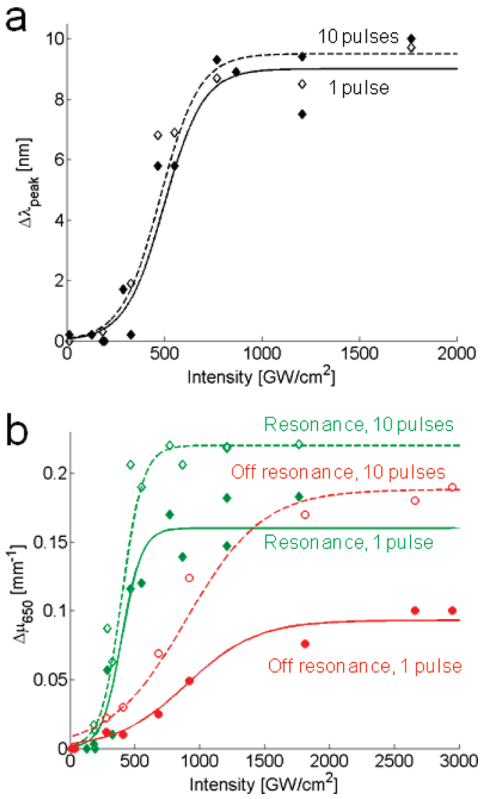

Figure 4. (a) Intensity-dependent peak extinction shifts for the GNP-45 solutions, following a single pulse (full diamonds) and 10 pulses (empty diamonds) at resonance wavelength (550 nm). (b) Extinction decrease at 650 nm (text) for the GNP-45 solution at resonance (diamonds) and off-resonance (circles) illuminated by a single pulse (full markers) and by 10 pulses (empty markers). Solid and dashed curves in (a) and (b) represent sigmoid trend line fits for the 1 and 10 pulse illuminations, respectively.

following the illumination of each pulse. To assess these changes, we have placed a 1 μL drop of each nanoparticle solution between the glass walls of a 600 μm thick glass cuvette. Because of the relatively high affinity of the liquid to the inner walls of the cuvette, each drop formed a nearly cylindrical shape with 600 μm height and approximately 800 μm diameter base. The drops were illuminated by a series of 1, 2, 5, and 10 pulses at 550 nm (resonance wavelength), with fluence of 75 mJ/cm^2 per pulse (1.5 TW/cm^2 peak intensity), and a beam diameter of 700 μm, sufficient for illuminating the entire volume of the drop. After each pulse sequence, the extinction spectrum was recorded and the solution was extracted from the cuvette for imaging by TEM. Particles from at least four different areas of each grid were imaged to reduce the possible effect of sample nonuniformity. Nearly 5000 particles were imaged for each experiment.

The effect of resonant illumination at 550 nm could be noticed by comparing the TEM images of the GNP-45 solution before illumination (part a of Figure 5), after 1 pulse (part b of 5), 2 pulses (part c of 5), and 10 pulses (part d of 5). Before illumination (part a of Figure 5), the solution contained mainly nanospheres, but also a certain quantity (approximately 20%) of different particle shapes, including triangles, rods, and icosahedrons.[36] After the first pulse illumination, a more homogeneous assortment of particles was observed, with a smaller abundance of nanorods and of other particles with sharper

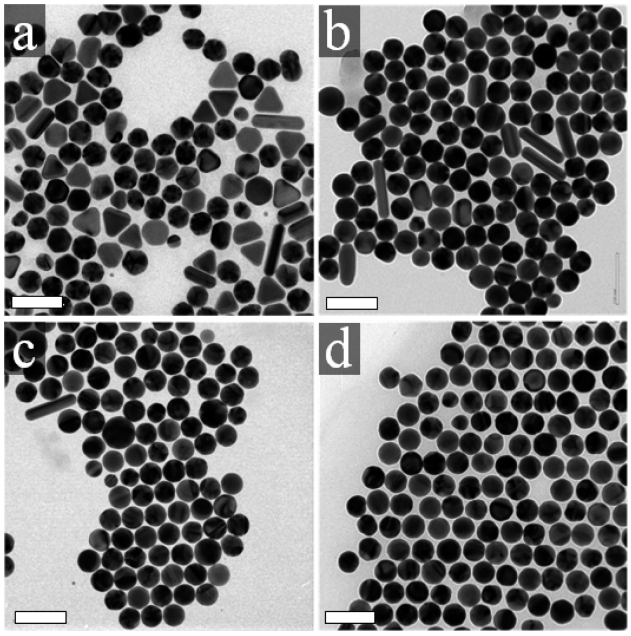

Figure 5. Typical transmission electron microscopy images of the GNP-45 solution (a) before illumination, and following (b) 1, (c) 2, and (d) 10 pulses at resonance wavelength. Scale bars represent 100 nm.

corners or edges (part b of Figure 5). This trend continued with each additional pulse (parts c and d of Figure 5), until almost all of the particles were transformed into spheres with a narrower size distribution. A similar effect was evident by visual examination of the TEM images of the resonantly illuminated drops from the GNP-23 and GNP-16 solutions (data not shown).

To better quantify these changes, we have developed dedicated computer software that automatically identifies individual particles in each TEM image and computes several morphological parameters for every particle in the 2D image. The most important parameters, summarized in Table 1, include the length of the particle's short axis, the length of its long axis, its effective diameter (calculated as the diameter of a perfect sphere with identical area), its aspect ratio, and the exclusive disjunction (XOR) between the particle shape and a perfect circle with the same effective diameter and the same center of mass. Owing to the large number of imaged particles, sampling errors were considerably smaller than the actual measurement errors, which were in the range of $\pm$2 nm due to the limited resolution of the TEM images and inaccuracies in the microscope's calibration.

Histograms of the calculated parameters extracted from GNP-45 solution without illumination (solid black lines), illuminated by 1 pulse (dashed blue lines) and illuminated by 10 pulses (dotted red lines), at resonance are shown in Figure 6. Approximately 2600 particles from each experiment were used for the statistical data. The histograms of the solutions that were illuminated by 2 and 5 pulses are not shown for brevity. The disappearance of nanorods and other nonspherical particles is clearly evident by examining the abundance of the XOR (part a of Figure 6) and the aspect ratio (part b of Figure 6) parameters. Lowest XOR values correspond to spherical particles, where higher values often correspond to prisms ($\sim$0.2) and rods (>0.3). The abundances of XOR values lower than 0.1 increase from 21% to 52% after the first pulse and up to 67% after 10 pulses. Similarly, the portion of particles having aspect ratios

Table 1. Definitions of the Five Morphological Parameters Used to Characterize the Nanoparticles

Symbol	Name	Definition
	Short axis	Shortest distance through the particle center.
	Long axis	Longest distance through the particle center.
d_s	Effective diameter	Diameter of a sphere with similar measured area S, $d_S = 2\sqrt{S/\pi}$.
AR	Aspect Ratio (AR)	Ratio between the short and the long axes.
	XOR	The normalized exclusive OR between the particle profile and a circle with diameter d_s.

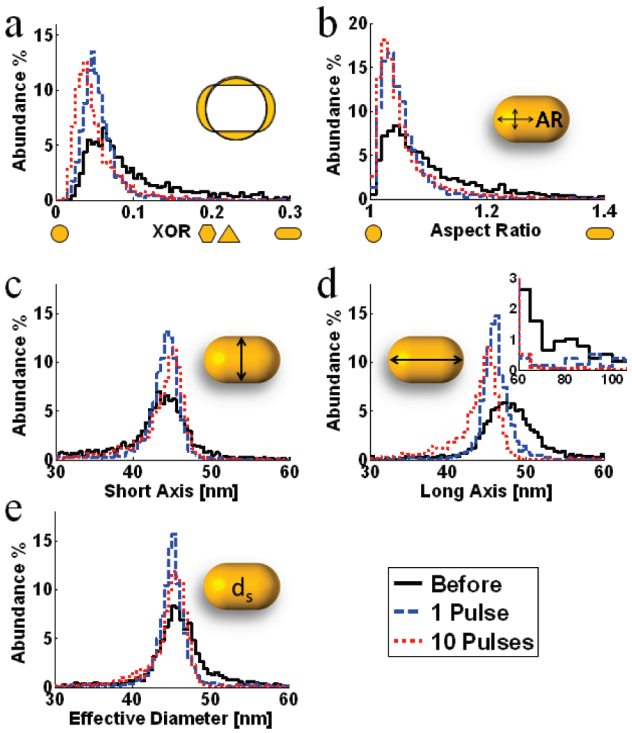

Figure 6. Histograms of the measured morphological parameters for the GNP-45 solution illuminated by 50 fs pulses at resonance 550 nm wavelength: (a) the XOR parameter, (b) aspect ratio, (c) short axis, (d) long axis, and (e) the effective diameter. Distributions before illumination, after a single pulse, and after 10 pulses are plotted by black solid line, blue dashed line, and red dotted line, respectively.

higher than 1.2 drops from 21% to 5% after the first pulse and down to 3% after 10 pulses (part b of Figure 6). These morphological parameter changes indicate the extinction of nonspherical particles and nanorods from the solution.

The tendency toward more homogeneous distribution of particles is also apparent when examining the abundances of

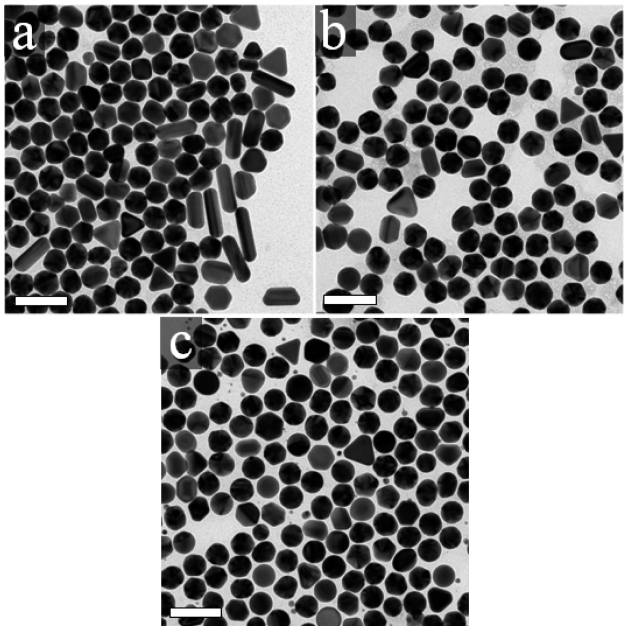

Figure 7. Typical transmission electron microscopy images of the GNP-45 solution (a) before illumination, and following (b) 1 and (c) 10 off-resonance (800 nm) pulses. Scale bars represent 100 nm.

the short axis (part c of Figure 6) and the long axis (part d of Figure 6) lengths. Following a single femtosecond pulse at resonance wavelength, both distributions show a nearly 2-fold narrowing. A similar effect was observed in the effective area diameter, d_S (part e of Figure 6). The disappearance of nanorods is also evident through the decrease of the percentage of particles with axes longer than 55 nm, which drops from 12% to 4% after the first pulse and down to 2% after 10 pulses (insert in part d of Figure 6). Because nanorods have their resonance wavelengths in the red and the near-infrared parts of the spectrum,[20] this observation agrees with the observed extinction reduction at this wavelength range (Figure 2).

Similar results to those presented in Figure 6 were obtained using resonance (550 nm) illumination of the GNP-23 and GNP-16 solutions, with the only difference being the smaller magnitudes of the observed changes. For all three solutions (data not shown), the nanoparticles population became more homogeneous after each pulse; the particles became more spherical, while keeping their average effective diameters (within the accuracy of the experimental system).

To examine morphological changes due to single pulses at off-resonance (800 nm) wavelength, we have applied a similar experimental protocol for illuminating the three solutions by 800 nm pulses having fluence of 0.15 J/cm^2 per pulse (3 TW/cm^2 peak intensity), 3-fold lower than the threshold for optical breakdown in water (10 TW/cm^2).[43] Typical TEM images of a portion from the GNP-45 solution before (part a of Figure 7), after a single pulse illumination (part b of Figure 7), and after 10 pulses (part c of Figure 7) show only minor visible differences in particle shapes; nanorods seem to have disappeared from the solution and a new type of small particles, of less than 20 nm in diameter, appeared at most of the images.

Histograms of the five morphological parameters (Table 1) of the GNP-45 solution, before (solid black lines, 2573 particles analyzed), after one 50 fs off-resonance pulse illumination (dashed blue lines, 1194 particles), and after 10 pulses (dotted

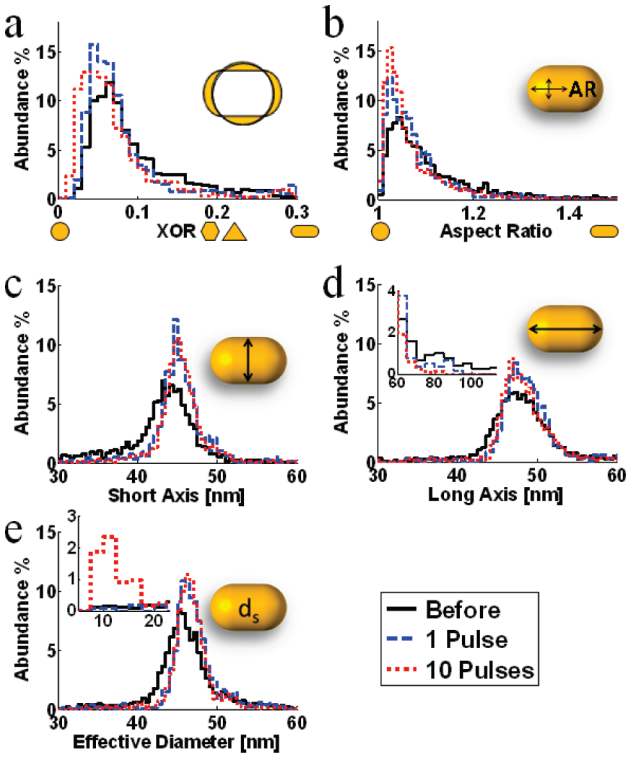

Figure 8. Histograms of the measured morphological parameters for the GNP-45 solution illuminated by 50 fs pulses at off-resonance 800 nm wavelength: (a) the XOR parameter, (b) aspect ratio, (c) short axis, (d) long axis, and (e) the effective diameter. Distributions before illumination, after a single pulse, and after 10 pulses are plotted by black solid line, blue dashed line, and red dotted line, respectively.

red lines, 1658 particles), are shown in Figure 8. The shape parameters XOR and aspect ratio, plotted in parts a and b of Figure 8 respectively show that most of the particles have kept their general shape. Most of the variations in the low XOR and aspect ratio values are attributed to the appearance of the small, sub-20 nm spherical particles (part c of Figure 7). Other particles such as prisms and icosahedrons were less affected and their abundance was kept nearly constant even after 10 pulses. Although the pulse intensity was nearly doubled compared with the intensity at the resonance illumination experiments, here the changes in the short axis, the long axis, and the effective diameter (parts c−e respectively of Figure 8) were less obvious: approximately 25% narrowing of the main abundance peak (compared to 45% narrowing in the resonance illumination) and statistically insignificant shifts of the main peaks toward larger values. More noticeable is the rapid decrease in the abundance of particles having axes longer than 55 nm (insert of part d of Figure 8), mostly attributed to nanorods, from 12% to 9% after the first pulse and to less than 5% after 10 pulses. Another significant effect is the 10-fold increase in the number of particles with effective diameters below 20 nm, from less than 0.5% in the original solution up to 5% after 10 pulses (insert of part e of Figure 8). Such an effect was not observed for resonance illumination.

All the statistically significant spectral and morphological changes following a single pulse illumination at resonance and off-resonance conditions are summarized in Table 2, which highlights the wide variety of the observed changes and emphasizes the differences between the two illumination wavelengths.

DISCUSSION

Illuminated by a single femtosecond pulse at resonance wavelength, gold nanoparticles were shown to undergo morphological changes that directly affect their optical properties. The very first 50 fs pulse at 550 nm caused a noticeable decrease of 2−5% in the peak extinction of all the three tested solutions. TEM images of the illuminated particles can only partially elucidate this effect by showing the disappearance of particles with sharp edges, which are characterized by higher light extinction than nanospheres. Another factor that may contribute to the light extinction decrease is the disintegration of small particle aggregates. Although significant aggregations in the tested solutions were not expected or observed during the process of sample preparation, some small aggregates may have formed during the experiment, increasing the light extinction primarily at the near-infrared part of the spectrum.

After the first pulse, each additional pulse at resonance wavelengths caused a slight (1−5%) increase in the peak extinction values (Figure 2), a trend which could be attributed to the increase in the total number of spherical (low XOR and aspect-ratio) particles (parts a and b of Figure 6 and parts a and b of Figure 8). Additional changes in the extinction spectra after each resonance pulse could be well explained by the visual inspection of the TEM images. First, the blue shifts in the extinction spectra, accompanied by a gradual decrease of the extinction at red wavelengths (up to the fifth pulse), could be attributed to the disappearance of particles with sharp corners or edges (parts a−d of Figure 5). Such particles are known to have red-shifted spectra due to the high order multipoles contribution to the total electromagnetic fields.[15,17] Second, the narrowing of the extinction spectra of all three solutions after each pulse (Figure 2) correlated well with the increased homogeneity of the solutions, as indicated by the narrowing of all the measured parameter distributions (Figure 6). Third, with the exception of the very first pulse, most of the observed effects were incremental as evident both from the spectral measurement and the TEM analysis. The gradual changes in particle morphology could be attributed to particle rotation between pulses, which would affect its orientation in space relative to the linear polarization of the pulses, and hence vary the magnitude of the effects between the particles.[25]

Perhaps unexpectedly, we could not identify any statistically significant decrease of the averaged particle's size. Whereas the spectral measurements showed slight blue shift, which may also indicate particle size reduction, detailed data analysis of all TEM images could not identify such an effect. Though numerous works have previously reported size reduction of nanoparticles illuminated by long series of nanosecond and picosecond pulses,[18−23] the effect of femtosecond pulses may be different in nature, causing no significant particle size reduction.

Using femtosecond pulses at off-resonance wavelength, the spectral and morphological changes were smaller and more gradual, although pulse energy was approximately 2-fold higher than that of the resonance experiment. The center wavelength and the width of the extinction spectra were not affected by the 50 fs, 800 nm pulses. Also, particles with sharp edges were still present even after 10 pulses. The most noticeable difference due to off-resonance illumination was the gradual elimination of nanorods from the initial solutions (approximately 12% of the particles). This effect was evident by the gradual decrease in the extinction spectra at long wavelengths, by visual inspection of the

Table 2. Summary of the Spectral and Morphological Changes Caused by a *Single Pulse* Illumination

illumination	morphological effect	extinction spectrum
single pulse, 550 nm (resonance)	loss of particles with sharp corners	blue shift
	loss of nanorods and high aspect ratio (AR > 1.1) particles	• lower peak extinction (after 1st pulse only)
		• lower extinction at red wavelengths
	higher concentration of nanospheres	higher peak extinction (after 2nd pulse)
	increased particle homogeneity	narrower spectrum
single pulse, 800 nm (off-resonance)	appearance of much smaller nanospheres	higher peak value
	loss of nanorods and high aspect ratio (AR > 1.5) particles	lower extinction at red wavelengths

TEM images (Figure 7), and by noting the disappearance of particles with long axis longer than 55 nm (the insert of part d of Figure 8). Here too, the gradual nature of the changes is attributed to the random, timely varying orientation of the nanorods with respect to the linear polarization of the light pulses. Another effect, which may be closely related to the disappearance of nanorods, was the appearance of new small particles with diameters between 8 and 18 nm (part c of Figure 7 and the insert of part e of Figure 8). Similar effects were previously reported following the resonance excitation of gold nanorods by long series femtosecond pulses.[20,28] These new particles are the main reason for the noticeable increase in the total number of spherical particles, characterized by low XOR and aspect-ratio parameters (parts a and b of Figure 8).

The physical interactions between gold nanoparticles and femtosecond pulses differ significantly from the interactions induced by pulse durations in the nanosecond range, primarily because of the different time scales involved in the transfer and the diffusion of energy. The process of photoexcitation in gold particles has a typical time scale of a few femtoseconds, whereas most other processes require longer periods of time: thermalization due to electron−electron interactions lasts several hundreds of femtoseconds, lattice heating by electron−phonon interactions requires several picoseconds, particle melting requires tens of picoseconds, and the diffusion of the absorbed heat to the surrounding medium requires several hundreds of picoseconds.[25,26] The different time scales allow simpler theoretical modeling of the various excitation and dissipation processes, and could provide better understanding of the various physical processes which are involved, including multiphoton absorption, plasma formation, nonthermal electron distribution, nonthermal melting, formation of highly energetic free electrons, and the ejection of metal ions from charged nanoparticles (often referred to as coulomb explosions).

In processes that do not involve loss of material (gold atoms or electrons) to the surrounding medium, most of the light energy absorbed by a nanoparticle during the pulse, eventually redistributes within the particle and could induce surface or bulk melting. The energies needed to melt a particle, according to the thermodynamical model described in refs 25,42,44 are 0.039 pJ, 0.28 pJ, and 2.5 pJ for the particles in the GNP-16, GNP-23, and the GNP-45 solutions, respectively. In our experiments, the energy absorbed from a single off-resonance (800 nm) pulse was approximately equal to the energy needed to melt the particle, and was 20 times higher than the melting energy for the resonance (550 nm) pulses, due to the higher absorption cross-section at resonance. Such large differences between the two excitation wavelengths suggest that entirely different physical mechanisms were involved in particle reshaping: at resonance, the pulses have enough energy to evaporate the particles or to ionize large number of electrons through multiphoton ionization, avalanched ionization, or thermionic emission.[43,44] The existence of well-defined threshold intensities, as evident from Figure 4 for all three solutions and for both excitation wavelengths, may imply the existence of such nonlinear physical process, or a combination of such processes.

CONCLUSIONS

The effect of a single femtosecond pulse on gold nanoparticles was studied using an experimental protocol that included measuring the optical extinction spectra, imaging large quantities of particles using TEM, and analyzing the resulting images by extracting key morphological parameters from the images. We have found that single resonance excitation pulses above a certain intensity threshold induce noticeable changes to nanoparticle solutions of various particle dimensions. At resonance wavelength, particles with sharp corners became spherical and kept their overall size after a single pulse, leading to more homogeneous solutions. While the size and shape of most particles were not affected following a single pulse at off-resonance wavelength, a new type of smaller spheres appeared, probably due to rapid defragmentation of high aspect ratio particles. We believe that by isolating the effect of a single pulse from the cumulative effect of a long series of pulses, the presented experimental data would assist in understanding the underlying processes of the interaction between noble-metal nanoparticles and intense optical pulses.

AUTHOR INFORMATION

Corresponding Author

*E-mail: yelin@bm.technion.ac.il.

ACKNOWLEDGMENT

The study was funded in part by the European Research Council starting grant (239986). The authors thank Dr. Dan Oron for assisting in nanoparticle preparation.

REFERENCES

(1) Huang, X.; Neretina, S.; El-Sayed, M. A. *Adv. Mater.* **2009**, *21*, 4880–4910.

(2) Lakowicz, J. *Plasmonics* **2006**, *1*, 5–33.

(3) Pelton, M.; Aizpurua, J.; Bryant, G. *Las. Phot. Rev.* **2008**, *2*, 136–159.

(4) Peleg, G.; Lewis, A.; Bouevitch, O.; Loew, L.; Parnas, D.; Linial, M. *Bioimaging* **1996**, *4*, 215–224.

(5) Wang, H.; Huff, T. B.; Zweifel, D. A.; He, W.; Low, P. S.; Wei, A.; Cheng, J.-X. *Proc. Natl. Acad. Sci. U.S.A.* **2005**, *102*, 15752–15756.

(6) Yelin, D.; Oron, D.; Thiberge, S.; Moses, E.; Silberberg, Y. *Opt. Express* **2003**, *11*, 1385–1391.

(7) Chan, W. C.; nbsp, W.; Nie, S. *Science* **1998**, *281*, 2016–2018.
(8) Kneipp, K.; Haka, A. S.; Kneipp, H.; Badizadegan, K.; Yoshizawa, N.; Boone, C.; Shafer-Peltier, K. E.; Motz, J. T.; Dasari, R. R.; Feld, M. S. *Appl. Spectrosc.* **2002**, *56*, 150–154.
(9) He, L.; Musick, M. D.; Nicewarner, S. R.; Salinas, F. G.; Benkovic, S. J.; Natan, M. J.; Keating, C. D. *J. Am. Chem. Soc.* **2000**, *122*, 9071–9077.
(10) Cheng, Y.; C. Samia, A.; Meyers, J. D.; Panagopoulos, I.; Fei, B.; Burda, C. *J. Am. Chem. Soc.* **2008**, *130*, 10643–10647.
(11) Fortina, P.; Kricka, L. J.; Graves, D. J.; Park, J.; Hyslop, T.; Tam, F.; Halas, N.; Surrey, S.; Waldman, S. A. *Trends Biotechnol.* **2007**, *25*, 145–152.
(12) Huang, X.; Jain, P.; El-Sayed, I.; El-Sayed, M. *Lasers Med. Science* **2008**, *23*, 217–228.
(13) Huang, X.; Qian, W.; El-Sayed, I. H.; El-Sayed, M. A. *Lasers Surg. Med.* **2007**, *39*, 747–753.
(14) Loo, C.; Lowery, A.; Halas, N.; West, J.; Drezek, R. *Nano Lett.* **2005**, *5*, 709–711.
(15) Kelly, K. L.; Coronado, E.; Zhao, L. L.; Schatz, G. C. *J. Phys. Chem. B* **2002**, *107*, 668–677.
(16) Messinger, B. J.; von Raben, K. U.; Chang, R. K.; Barber, P. W. *Phys. Rev. B* **1981**, *24*, 649.
(17) Shuford, K. L.; Ratner, M. A.; Schatz, G. C. *J. Chem. Phys.* **2005**, *123*, 114713–114719.
(18) Amendola, V.; Meneghetti, M. *J. Mat. Chem.* **2007**, *17*, 4705–4710.
(19) Kamat, P. V.; Flumiani, M.; Hartland, G. V. *J. Phys. Chem. B* **1998**, *102*, 3123–3128.
(20) Link, S.; Burda, C.; Nikoobakht, B.; El-Sayed, M. A. *J. Phys. Chem. B* **2000**, *104*, 6152–6163.
(21) Muto, H.; Miyajima, K.; Mafune, F. *J. Phys. Chem. C* **2008**, *112*, 5810–5815.
(22) Takami, A.; Kurita, H.; Koda, S. *J. Phys. Chem. B* **1999**, *103*, 1226–1232.
(23) Werner, D.; Hashimoto, S.; Tomita, T.; Matsuo, S.; Makita, Y. *J. Phys. Chem. C* **2008**, *112*, 16801–16808.
(24) Yamada, K.; Tokumoto, Y.; Nagata, T.; Mafune, F. *J. Phys. Chem. B* **2006**, *110*, 11751–11756.
(25) Ekici, O.; Harrison, R. K.; Durr, N. J.; Eversole, D. S.; Lee, M.; Ben-Yakar, A. *J. Phys. D* **2008**, *41*, 185501.
(26) Rethfeld, B.; Sokolowski-Tinten, K.; von der Linde, D.; Anisimov, S. I. *Appl. Phys. A: Mater. Sci. Process.* **2004**, *79*, 767–769.
(27) Vogel, A.; Noack, J.; Hüttman, G.; Paltauf, G. *Appl. Phys. B: Lasers Opt.* **2005**, *81*, 1015–1047.
(28) Besner, S.; Kabashin, A.; Winnik, F.; Meunier, M. *Appl. Phys. A: Mater. Sci. Process.* **2008**, *93*, 955–959.
(29) Besner, S.; Kabashin, A. V.; Meunier, M. *Appl. Phys. A: Mater. Sci. Process.* **2007**, *88*, 269–272.
(30) Csaki, A.; Garwe, F.; Steinbruck, A.; Maubach, G.; Festag, G.; Weise, A.; Riemann, I.; Konig, K.; Fritzsche, W. *Nano Lett.* **2007**, *7*, 247–253.
(31) Eversole, D.; Luk'yanchuk, B.; Ben-Yakar, A. *Appl. Phys. A: Mater. Sci. Process.* **2007**, *89*, 283–291.
(32) Nedyalkov, N. N.; Takada, H.; Obara, M. *Appl. Phys. A: Mater. Sci. Process.* **2006**, *85*, 163–168.
(33) Plech, A.; Leiderer, P.; Boneberg, J. *Las. Phot. Rev.* **2009**, *3*, 435–451.
(34) Préz-Juste, J.; Pastoriza-Santos, I.; Liz-Marzán, L. M.; Mulvaney, P. *Coord. Chem. Rev.* **2005**, *249*, 1870–1901.
(35) Shoji, M.; Miyajima, K.; Mafune, F. *J. Phys. Chem. C* **2008**, *112*, 1929–1932.
(36) Gao, J.; Bender, C. M.; Murphy, C. J. *Langmuir* **2003**, *19*, 9065–9070.
(37) Jana, N. R.; Gearheart, L.; Murphy, C. J. *Langmuir* **2001**, *17*, 6782–6786.
(38) Mie, G. *Annalen der Physik* **1908**, *330*, 377–445.
(39) Quinten, M. *Appl. Phys. B: Lasers Opt.* **2001**, *73*, 245–255.
(40) Talley, C. E.; Jackson, J. B.; Oubre, C.; Grady, N. K.; Hollars, C. W.; Lane, S. M.; Huser, T. R.; Nordlander, P.; Halas, N. J. *Nano Lett.* **2005**, *5*, 1569–1574.
(41) Inasawa, S.; Sugiyama, M.; Yamaguchi, Y. *J. Phys. Chem. B* **2005**, *109*, 3104–3111.
(42) Link, S.; El-Sayed, M. A. *J. Chem. Phys.* **2001**, *114*, 2362–2368.
(43) Vogel, A.; Noack, J.; Nahen, K.; Theisen, D.; Busch, S.; Parlitz, U.; Hammer, D. X.; Noojin, G. D.; Rockwell, B. A.; Birngruber, R. *Appl. Phys. B: Lasers Opt.* **1999**, *68*, 271–280.
(44) Pyatenko, A.; Yamaguchi, M.; Suzuki, M. *J. Phys. Chem. C* **2009**, *113*, 9078–9085.